

# RSC Advances



This is an *Accepted Manuscript*, which has been through the Royal Society of Chemistry peer review process and has been accepted for publication.

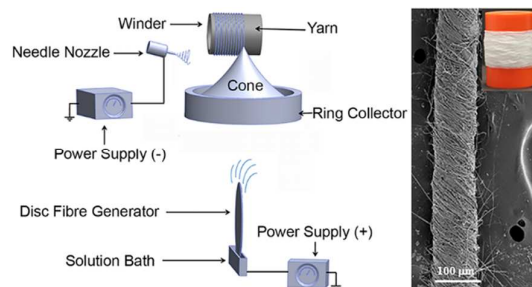
*Accepted Manuscripts* are published online shortly after acceptance, before technical editing, formatting and proof reading. Using this free service, authors can make their results available to the community, in citable form, before we publish the edited article. This *Accepted Manuscript* will be replaced by the edited, formatted and paginated article as soon as this is available.

You can find more information about *Accepted Manuscripts* in the [Information for Authors](#).

Please note that technical editing may introduce minor changes to the text and/or graphics, which may alter content. The journal's standard [Terms & Conditions](#) and the [Ethical guidelines](#) still apply. In no event shall the Royal Society of Chemistry be held responsible for any errors or omissions in this *Accepted Manuscript* or any consequences arising from the use of any information it contains.

## TOC

A hybrid needle-needleless electrospinning technique has been developed to directly convert polymer solution into a highly-twisted, continuous nanofibre yarn.



## ARTICLE

## Highly-twisted, Continuous Nanofibre Yarns Prepared by a Hybrid Needle-Needleless Electrospinning

Cite this: DOI: 10.1039/x0xx00000x

Nadeem Shuakat, Tong Lin\*

Received 00th January 2015,  
Accepted 00th January 2015

DOI: 10.1039/x0xx00000x

www.rsc.org/

Nanofibres prepared by electrospinning have shown enormous potential for various applications. They are obtained predominantly in the form of nonwoven fibre webs. The 2-dimensional nonwoven feature and fragility have considerably confined their further processing into fabrics through knitting or weaving. Nanofibre yarns, which are nanofibre bundles with continuous length and twist feature, show improved tensile strength, offering opportunities for making 3-dimensional fibrous materials with precisely controlled fibrous architecture, porous feature and fabric dimension. Despite a few techniques have been developed for electrospinning nanofibre yarns, they are chiefly based on needle electrospinning technique, which often has low nanofibre productivity. In this study, we for the first time report a nanofibre yarn electrospinning technique which combines both needle and needleless electrospinning. A rotating intermediate ring collector was employed to directly collect freshly-electrospun nanofibres into a fibrous cone, which was further drawn and twisted into a nanofibre yarn. This novel system was able to produce high tenacity yarn (tensile strength 128.9 MPa & max strain 222.1%) at a production rate of 240 m/h, with a twist level up to 4,700 twists per metre. The effects of various parameters, e.g. position of the electrospinning units, operating conditions and polymer concentration, on nanofibre and yarn production were examined.

### Introduction

Nanofibres show large surface-to-mass (or volume) ratio, high porosity with excellent pore-interconnectivity, and remarkable physiochemical property. These features considerably enhance the applications in the fields of filtration<sup>1</sup>, sensors<sup>2-4</sup>, biomedical<sup>5,6</sup>, protective clothing<sup>7,8</sup>, catalysis, and energy generation and storage<sup>9-11</sup>. Different techniques have been available for making nanofibres, such as drawing<sup>12</sup>, template synthesis<sup>13</sup>, phase separation<sup>14-16</sup>, centrifugal-spinning<sup>17,18</sup>, micro fibre extrusion<sup>19-21</sup>, solution blowing<sup>22-24</sup>, chemical vapour deposition<sup>25-27</sup> and hydro-thermal<sup>28-30</sup>. However, electrospinning stands distinct to the others in its simplicity, cost effectiveness, control-ability and capability to large-scale production.

Electrospinning involves using a high electric field to directly convert a polymer fluid into fine solid fibres. During electrospinning, a polymer solution is charged with a high voltage. A Taylor cone develops on the polymer solution surface. When the applied voltage is above a critical value, the electric force overcomes the surface tension of the solution, leading to jet initiation on the apex of the Taylor cone. The charged jet then undergoes an intensive interaction with the electric field and meanwhile charges repel within the jet, stretching itself thinner. Solvent evaporation from the filament results in dry fibres. Most of the nanofibres produced by electrospinning are in the form of randomly-orientated

nonwoven mats, which are fragile and hard to control the fibrous structure.

Recently, considerable efforts have been devoted to making nanofibre yarns through electrospinning, and exploring the novel applications<sup>31,32</sup>. Yarns are linear assemblies of fibres with improved cohesiveness among the fibres and increased mechanical properties through twisting. Nanofibre yarns offer opportunities to prepare complex fibrous structures using conventional weaving, knitting or embroidery techniques.

Three main strategies have been developed to prepare nanofibre yarns directly through electrospinning<sup>33,34</sup>, including 1) depositing nanofibres into a non-solvent liquid<sup>35-38</sup>, 2) drawing and twisting nanofibres from a motionless intermediate collector<sup>39-41</sup>, and 3) directly drawing from a rotating fibrous cone<sup>42-45</sup>. With the non-solvent deposition method, an additional drying process is required, and improper twists often result. Drawing and twisting nanofibres from a still collector suffers from yarn evenness and frequent damage. The rotating fibrous cone method shows high twist level, yarn evenness and continuity<sup>42,43</sup>. However, almost all yarn electrospinning techniques are based on needle electrospinning which uses need like nozzle to generate nanofibres. Needle electrospinning typically has limited fibre productivity due to each needle nozzle normally producing just one jet each time though it has advantages in producing multi-component nanofibres and tailoring fibre component, surface morphology, chemical composition and functionality.

Recently, needleless electrospinning appears as an alternative electrospinning technology showing much increased productivity because a large number of jets can be generated simultaneously from the limited space of the fibre generator<sup>46-53</sup>. Nanofibre yarns production using needleless electrospinning is expected to have higher productivity than that using needle electrospinning. However, needleless electrospinning is harder to manipulate in comparison to needle electrospinning, due to the higher applied voltage and multiple jets. Recently, Pokorny et al.<sup>54</sup> reported the formation of nanofibre yarn on a special needleless electrospinning driven by AC voltage. Nanofibre yarns produced by DC electrospinning have not been proven.

In this study, we for the first time develop a novel hybrid yarn electrospinning technique by combining needle electrospinning and needleless electrospinning. A disc-based fibre generator was chosen for needleless electrospinning because it is easy to operate at a relatively low applied voltage. A rotating intermediate ring collector was employed to directly collect nanofibres into a fibrous cone, which was further drawn and collected into a nanofibre yarn. Poly(vinylidene fluoride-co-hexafluoropropylene) (PVDF-HFP) was chosen as model polymer to prepare nanofibre yarns and elucidate the effect of various parameters on fibre/yarn formation because of its good electrospinning ability. This system was able to produce nanofibre yarns at a production rate of 240 m/h, with a twist level up to 4,766 twist per metre. Effects of setup dimension, processing parameters and polymer concentration on nanofibre and yarn formation were examined. The novel hybrid yarn electrospinning allows combination of the advantages from both electrospinning techniques to prepare composite nanofibre yarns with various novel functions.

## Experimental

**Materials:** Poly(vinylidene fluoride-co-hexafluoropropylene) (PVDF-HFP), dimethylformamide (DMF) and acetone were purchased from Sigma-Aldrich and used as received. A solvent mixture of acetone and DMF (1:1 vol/vol) was used to prepare PVDF-HFP solutions.

**Electrospinning of nanofibre yarns:** A purpose-built electrospinning setup was used to prepare nanofibre yarns. The setup comprised two electrospinning systems (one using needle nozzle and another needleless electrospinning), an intermediate ring collector, and a winder as schematically shown in Fig. 1a. The disc generator and the needle nozzle were separately connected to a positive high-voltage power supply (RR100-2P/240, Gamma High Voltage Research 0~100 kV) and a negative high-voltage power supply (ES30P, Gamma High Voltage Research 0~50 kV), respectively. The ring collector was mounted horizontally on a plastic board through a ball bearing to lower friction in rotation. A variable speed motor was connected to the ring collector through an O-ring belt. Disc produced nanofibres upwards, while the needle nozzle which was placed

near the ring collector produced nanofibres from top. The nanofibres were initially deposited on the rotary ring collector to form a fibrous web on the ring aperture. By manually dragging this web using a plastic rod, an inverted fibrous cone was generated, and a yarn was drawn endlessly from the apex of the cone.

**Characterizations:** Fibre and yarn morphologies were observed under a scanning electron microscope (SEM) (Neoscope). Nanofibre and yarn diameters were measured based on SEM images using an image analysis software (ImageJ1.46 r). Over 100 reads from different places were used for each measurement. Mechanical properties were examined on Favimat + (AI) Robot2. Five samples of each specimen were tested with a cross head speed of 10 mm and a gauge length of 10 mm.

## Results and discussion

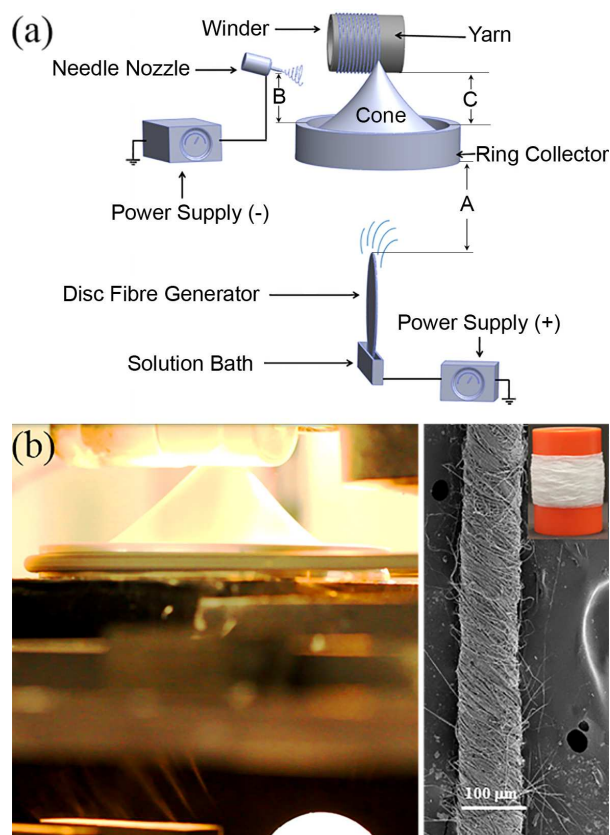


Fig. 1 a) Schematic illustration of yarn electrospinning setup, b) fibrous cone formed on top of ring collector, and c) SEM image of an electrospun nanofibre yarn (inset shows nanofibre yarn collected on a spool).

Fig. 1a schematically illustrates the setup for electrospinning of nanofibre yarns. Both needle and needleless electrospinning techniques were employed for the yarn preparation. The polymer solution was fed separately to the needle nozzle and the solution bath underneath the disc generator (though a syringe pump). The ring collector was set horizontally between the disc and the winder. When the needle and the disc electrospinning systems were run at applied

voltages of above 9 kV and 50 kV, respectively, while the disc rotated continuously at a speed 20 rpm, fibres were electrospun from the two systems, which deposited on the ring collector.

The key step to prepare nanofibre yarn using this hybrid electrospinning is the formation of a stable fibrous cone on the ring collector. Since the two electrospinning systems were charged by two power supplies with opposite polarity, the nanofibres produced from the two nanofibre generators should have different polarities. During electrospinning, when the ring collector rotated, a flat fibrous web was initially formed on the ring collector. Drawing the fibrous web from the central part of the fibrous web led to the formation of an inverted fibrous cone (Fig. 1b). Once a stable cone was formed, continuously drawing fibres from the apex of the fibrous cone led to formation of a continuous filament bundle. Twists were inserted into the fibre bundle because of the rotation of the fibrous cone with the ring collector. As result, a continuous yarn was formed and collected by the winder.

The fibre bundle shows a typical yarn morphology under SEM, and fibres in the yarns looked uniform with an average diameter of 845 nm (Fig. 1c). To prepare a fibrous web on the ring collector, it is essential for both needle and needleless electrospinning systems to work simultaneously. When only one of the fibre generators worked, the fibres prepared adhered mainly on the inner wall of the ring collector without forming a fibrous web.

The position of different elements in the yarn electrospinning setup greatly affected nanofibre deposition,

formation of fibrous cone, cone stability, and final nanofibre yarn. Fig. 1a also depicts important dimensions between various elements, among which the relative positions between the fibre generators and ring collector were crucial for yarn electrospinning.

Table 1 summarizes the effect of nanofibre generator locations on the stability of fibrous cone and yarn formation. It was important to position the disc generator beneath the centre of the ring collector. In this way, the nanofibres were deposited evenly on the ring collector. Unsymmetrical distribution of nanofibres resulted when the disc generator was placed beyond the central line of the ring collector, which led to unstable cone.

The distance between the disc and the ring collector played a key role in deciding the yarn formation. When the distance was less than 30 mm, wet fibres formed, which struck inside the ring collector. As a result, no fibrous cone and nanofibre yarn were prepared. Thin fibrous cone and discontinuous yarn could be obtained when the disc-ring distance was between 31 mm to 49 mm. In this case, most of the fibres were found to be fused together. When the distance was in the range of 50 mm to 60 mm, a continuous cone and incessant yarn was formed. Further increasing the distance beyond 61 mm resulted in thinner cone and frequent yarn breakage. At such a high distance, lots of nanofibres flew into air, leaving only a small amount of nanofibres to add onto the fibrous cone. However, no cone or yarn was produced when the disc-ring distance was larger than 72 mm.

Table 1 Effect of nanofibre generators and winder position on cone stability and yarn formation

Conditions	Disc-ring* (mm)	Needle-ring** (mm)	Winder-ring*** (mm)	Cone	Yarn
<b>A 1</b>	<30	48	55	No cone	No yarn
<b>A 2</b>	31 ~ 49	48	55	Unstable, wet	Discontinuous
<b>A 3</b>	50 ~ 60	48	55	Stable, dry	Continuous
<b>A 4</b>	61 ~ 68	48	55	Unstable, dry	Discontinuous
<b>A 5</b>	> 72	48	55	No cone	No yarn
<b>B 1</b>	60	< 25	55	No cone	No yarn
<b>B 2</b>	60	26 ~ 40	55	Unstable, wet	Discontinuous
<b>B 3</b>	60	41 ~ 50	55	Stable, dry	Continuous
<b>B 4</b>	60	51 ~ 66	55	Unstable, dry	Discontinuous
<b>B 5</b>	60	> 67	55	No cone	No yarn
<b>C 1</b>	60	48	<25	No cone	No yarn
<b>C 2</b>	60	48	26 ~ 49	Unstable, wet	Discontinuous
<b>C 3</b>	60	48	50 ~ 59	Stable, dry	Continuous
<b>C 4</b>	60	48	60 ~ 66	Unstable, dry	Discontinuous
<b>C 5</b>	60	48	> 67	No cone	No yarn

\* Disc was placed perpendicularly below ring collector;

\*\* Needle generator was positioned at angle of 30° and 20 mm from inner ring centre;

\*\*\* Drum winder was placed in centre directly above the ring collector.

Fig. 2 shows the effect of disc-ring distance on fibre and yarn diameters. With increasing the distance, the yarn diameter increased initially until the distance reached 60 mm. The yarn diameter then decreased rapidly with further increasing the distance. This decrease in yarn diameter can be explained by that fibres electrospun at a long distance are easy to escape into air, instead of depositing onto the fibrous cone. In contrast, nanofibre diameter decreased gradually with the increase in disc-ring distance. When the distance was larger than 60 mm, the fibre diameter showed a slight increase with increasing the distance, attributive to the reduced electric field.

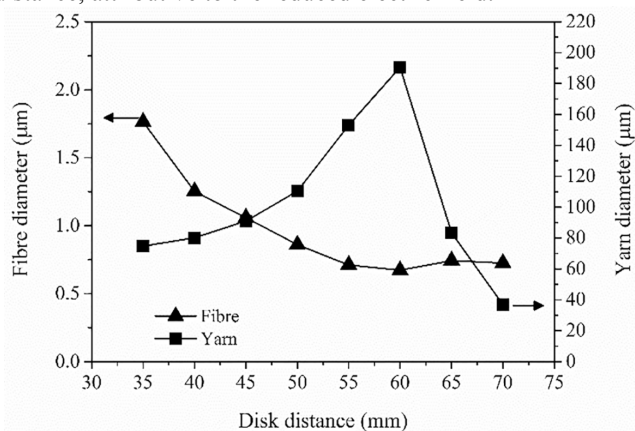


Fig. 2 Effect of disc-ring distance on fibre and yarn diameters.

Apart from the disc-ring distance, the position between the needle generator and the ring collector was also important to affect the yarn formation. Here, the needle nozzle was placed at an angle of  $30^\circ$  and 20 mm from ring centre. At this setting, nanofibres generated by the needle where equally deposited over the span between ring and winder.

Table 1 also gives details about the effect of needle-ring distance on fibre morphology, cone stability and yarn formation. When the distance was below 25 mm, all the fibres generated by the needle nozzle deposited on ring edge, and no fibrous web was formed on ring opening. When the distance was in the range of 26 ~ 40 mm, intermittent wet cone was formed, but still no continuous yarn was prepared. When the distance was larger than 41 mm, stable cone and continuous yarn were formed. At this point, the jets from the needle nozzle moved towards the gap between the winder and the ring collector. When the distance was beyond 51 mm, the majority of fibres were deposited on the winder, and only a very small number of fibres went to gap between the winder and the ring collector. Consequently, the cone became unstable and yarn ruptured frequently. When the distance was larger than 67 mm, the fibres started depositing on winder and no cone or yarn was formed.

In addition, the ring-winder distance also affected cone and yarn formation. When winder was placed less than 25 mm away from the ring collector, wet nanofibres were generated from the needle nozzle and deposited on the winder. In this case, neither fibrous cone nor yarn was produced. When the distance was in the range between 26 mm and 49 mm, fibres

deposited partly on ring and partly on winder, still no cone or yarn was formed. At a distance of 50 mm, fibres from needle generator accumulated on gap between the winder and the ring collector. At this stage, a very stable cone was formed and a continuous yarn could be drawn. When the winder-ring distance was larger than 60 mm, the cone frequently ruptured and discontinuous yarn was produced. Larger distance beyond 67 mm disturbed the balance between nanofibre generation, cone formation and yarn drawing. As result, no cone and yarn were formed.

The disc size and material were found to affect yarn formation and morphology. To examine the effect of disc size, four discs with different diameters (50 mm, 60 mm, 70 mm and 80 mm) and the same thickness 1 mm were employed. When disc size was 50 mm, fewer jets were generated resulting in wet and coarser fibres. These wet fibres were sticky and hard to form a continuous cone. Therefore, discontinues yarn was produced. Numerous dry fibres were produced on the disc with larger diameter. As a result, a stable cone and continuous yarn was formed. Fig. 3a shows the effect of disc diameter on fibre and yarn diameters. Increasing the disc diameter led to decrease in nanofibre diameter but increase in yarn diameter. The nanofibres of the smallest diameter were observed from 80 mm diameter disc, while the finest yarn was fabricated from 50 mm disc. The yarn produced from 80 mm disc was almost 4 times larger in diameter than that from 50 mm disc.

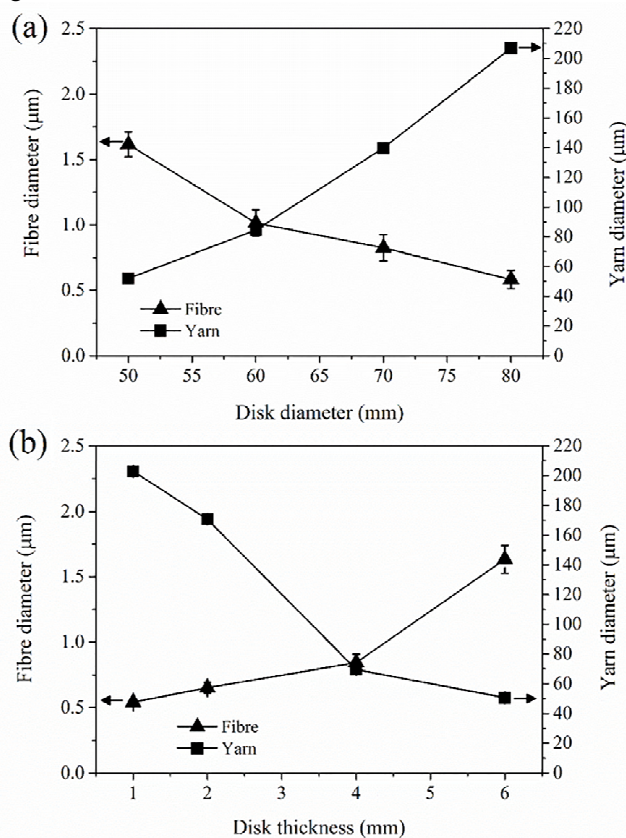


Fig. 3 Dependence of nanofibre and yarn diameters on a) disk diameter and b) disc thickness.

Disc thickness also showed a direct influence on fibres and yarn formation. When disc diameter was fixed at 80 mm and disc thickness was changed from 1 mm, 2 mm to 4 mm and 6 mm, both yarn and fibre diameter changed noticeably. As shown in Fig. 3b, with increasing the disc thickness, the fibre diameter increased, while the yarn diameter declined. This can be explained by the effect of disc thickness on electric field profile. It is reported that thinner discs showed higher electric field intensities at top of disc<sup>55</sup>.

In addition to the diameters, the yarn production was also affected greatly by the disc thickness. The thinner disc produced dry, finer fibres which could form a stable cone and continuous yarn easily, while fibres generated by the thicker disc were wet and coarse, which was hard to form stable cone and intermittent yarn. The disc material was another factor which was investigated for the nanofibre generation and yarn formation. Discs (80 mm diameter and 1 mm thickness) made of steel, aluminium, copper and high density polyethylene (HDP) were tested. At a low voltage, all the discs were able to produce nanofibres. However, when the voltage was above 50 kV, a corona discharge took place on the metal discs. In contrast, the HDP disc could produce nanofibres without corona discharge even when the applied voltage was 65 kV. The jets produced on non-conductive disc were numerous, continuous and equally distributed on disc surface. Conversely, the jet formation on the metal discs was irregular, discontinuous and scattered over disc surface. This suggested that the conductivity of disc affected the needleless electrospinning process.

Table 2, Effect of polymer concentration on yarn electrospinning\*

C %	$V_T$ kV	$V_w$ kV	Fibres	Stability	Yarns
9.0	23	38	Fused	Occasional cone	Discrete
11.0	25	42	Round beaded	Highly unstable	Discrete
13.0	27	45	Spindle beaded	Unstable	Discrete
15.0	30	50	Bead free	Stable	Continuous
17.0	34	54	Bead free	Unstable	Discrete
19.0	37	57	Bead free	Highly unstable	Discrete

\*Where  $V_T$  and  $V_w$  represent threshold voltage and working voltage respectively. Applied voltage and polymer concentration of solution for needle electrospinning were kept at 9 kV and 17.0 %, respectively. Disc, needle and winder were placed from ring collector at a distance of 60 mm, 48 mm and 55 mm, respectively.

Similar to conventional electrospinning, this yarn electrospinning was greatly affected by polymer concentration. To elucidate the effect of polymer concentration on fibre and yarn morphologies, solutions with a PVDF-HFP concentration from 9.0% to 19.0% were electrospun. Table 2 summarizes the effect of polymer concentration on threshold voltage for electrospinning, cone stability, fibre morphology, and yarn

continuity. When polymer concentration was in the range of 9.0% ~ 11.0%, a large number of jets could be seen at a voltage as low as 23 ~ 25 kV. Though at a voltage of 38 ~ 42 kV can run electrospinning smoothly, fibrous cone was difficult to produce due to wet fibres produced. When the polymer concentration was increased to 13.0 %, cone stability improved and yarn was easy to produce, still the yarn fabrication was discontinuous. The 15.0% polymer solution led to a steady cone and incessant yarn production. At higher polymer concentrations (e.g. above 17.0%), higher voltage was required to generate fibres. However, no continuous yarn was prepared because fibres produced had a lot of solvent rich areas and were not enough fibres to form a fibrous cone.

Fig. 4 shows effect of polymer concentration on fibre and yarn diameters. Beaded fibres were produced at a low concentration. Increasing the polymer concentration reduced fibre beads and fused fibrous morphology, yet coarser fibres were produced. Bead free fibres were obtained when the polymer concentration was over 15.0%. However, increasing the polymer concentration increased the threshold voltage to run electrospinning.

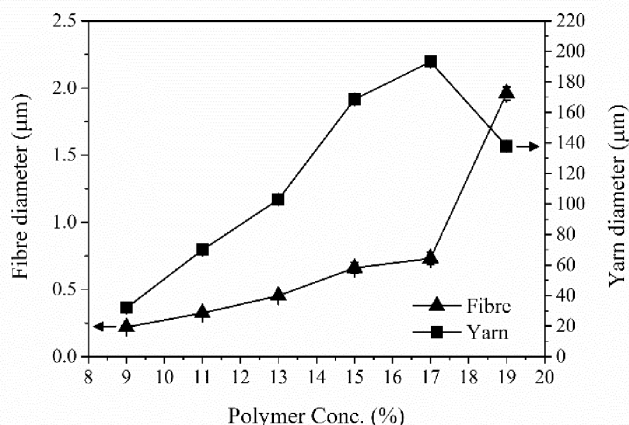


Fig. 4 Effect of polymer concentration on fibre and yarn diameters.

With increasing the polymer concentration to 13.0%, polymer viscosity increased and the solution layer on the disc was slightly thicker. On applying voltage above 45 kV, semi-continuous jets were produced from disc surface and dry fibres with smaller beads were observed. At this point, cone stability showed a little improvement, still yarn fabrication was not continuous. The 15.0% polymer solution showed increased viscosity and uniform thick polymer coverage on disc. At a voltage of 50 kV, the jet protrusion was distributed thoroughly on disc surface. The fibres produced from this solution were dry and bead-free, which led to a steady cone and incessant yarn production. At higher polymer concentrations (17.0% and above), polymer viscosity was so high that higher threshold voltage (34 ~ 37 kV) was required to generate nanofibres. As a result, steady production of nanofibres required higher voltage (54 ~ 57 kV), no enough fibres were generated to support the formation of cone and continuous yarn. Yarn diameter initially showed an increased trend with increasing the polymer concentration, and then declined. At a low polymer

concentration, wet fibres and fused fibrous structure led to small yarn diameter. This effect diminished with the increase in polymer concentration. The decrease in yarn diameter at a high concentrations was attributed to the difficulty in electrospinning.

Applied voltage on disc system plays a pivotal role in nanofibre and yarn production. The threshold voltages for electrospinning ( $V_{Threshold}$ ) and for the formation of fibrous cone ( $V_{working}$ ) are listed in Table 2. By keeping all other parameters unchanged, while adjusting the applied voltage on disc system, nanofibre generation and yarn formation were observed. No jets or fibres were produced when the voltage was below 30 kV. When the voltage was just above 30 kV, only a few jets appeared, but the fibres formed were wet and coarse. Occasionally, wet cone was formed which led to discontinuous yarn production. The solvent enriched fibres continued to produce even up to 40 kV. Fibrous cone formed by wet fibres was unstable and yarn broke occasionally during drawing due to the fused fibrous structure.

Once the voltage was above 45 kV, dry fibres were produced. Increasing the voltage decreased the number of fused fibres. When the voltage was increased to 50 kV, plenty of dry nanofibres were produced which formed steady fibrous cone and continuous yarn. Further increasing the voltage to 60 kV, a huge number of fibres were produced. However, a large number of fibres flew in all direction other than the target, and the fibres which reached target firmly affixed to the ring collector. As a result, cracked cone and discontinuous yarn resulted.

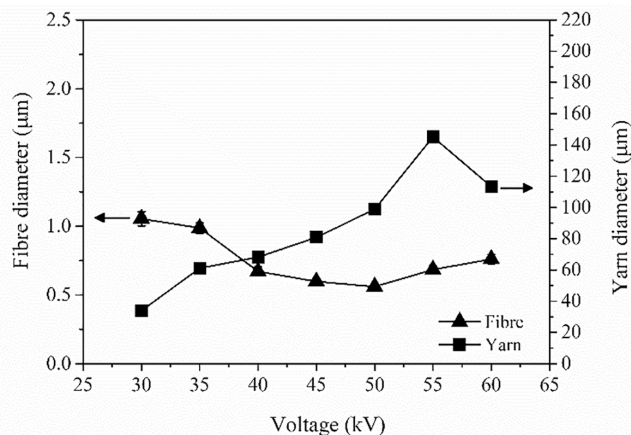


Fig. 5 Effect of applied voltage on fibre and yarn diameters.

Fig. 5 shows the effect of the applied voltage of the disc system on fibre and yarn diameters. With increasing the voltage, fibre diameter decreased initially until the voltage reached 50 kV. This could be attributed to the unconfined polymer supply from disc surface to electrospinning zone. At low applied voltage ( $\leq 45$  kV), fewer, random and coarser jets formed on disc surface forming wet fibres, resulting in low diameter yarn with fused structure. On gradually increasing applied voltage 50 kV, numerous, thinner, and equally distributed jets were formed on disc surface. The fibres produced at these higher voltages were thinner, dry and

completely separated from each other. The yarns produced from these dry, fine and well separated fibres showed larger diameters. Further increase in applied voltage ( $55 \text{ kV} \geq$ ), the jet stability and continuity was disturbed. In addition, majority of the fibres either went off target or firmly stuck to inner ring wall. Consequently, the yarns produced on such high voltages showed discontinuity in production and declining trend in diameter.

In this setup, only the polymer flow in needle generator was controlled through micro-syringe pump due to the flow rate in needleless system was not controllable parameter. Since polymer solution is uploaded onto the disc through disc rotation, the disc rotation speed should have an influence on yarn spinning. When the disc speed was in the range of 20~25 rpm, polymer solution was evenly loaded on disc surface. The jets were produced evenly from the top rim of the disc. At lower speed ( $\leq 15$  rpm), uneven coating was observed, while at higher speed ( $\geq 30$  rpm) polymer solution was thrown away from disc surface.

The flow rate on the needle system was also important to get neutral web over the ring collector. When the flow rate from needle generator was  $\leq 1.5$  ml/h, fibres were not enough to be produced from needle nozzle. The web was highly charged and could not form a fibrous cone. When the flow rate was increased to 2.5 ml/h, sufficient amount of fibres led to formation of a stable cone on the ring collector, which resulted in continuous nanofibre yarn formation. However, liquid dropping took place when the flow rate was higher than 3.0 ml/h. The cone from these fibres, frequently suffered splitting and adversely affected yarn formation.

Based on the ring rotation speed and the winding rate, twist level on the yarn can be estimated by the equation (1)

$$\text{Twist level (tpm)} = \frac{N_R}{S_w} \quad (1)$$

where  $N_R$  is the rotation speed of the ring collector in rpm (revolutions per minute) and  $S_w$  is winder speed in m/min (metres per minute). By varying the ring speed, twist levels can be adjusted. At a ring rotation speed below 310 rpm, the fibrous cone became unstable. When the ring speed increased to 440 rpm, stable fibre cone resulted, which can be drawn continuously into a nanofibre yarn. Cone stability and continuous yarn winding were not disturbed till the ring collector speeds were between 440 rpm to 1,430 rpm. However, ring collector speeds beyond 1500 rpm caused vibrations in overall system frequent cone cracking and ceasing nanofibre yarn production. With increasing ring collector speed within 440 ~ 1430 rpm, a steady increase in yarn twist levels was observed (as shown in Fig. 6). A maximum twist level of 4,766 twists per metre could be achieved from this modified nanofibre yarn electrospinning system. At this maximum twist level, highest twist angle of fibres along yarn was noticed to be  $48.8^\circ$ .

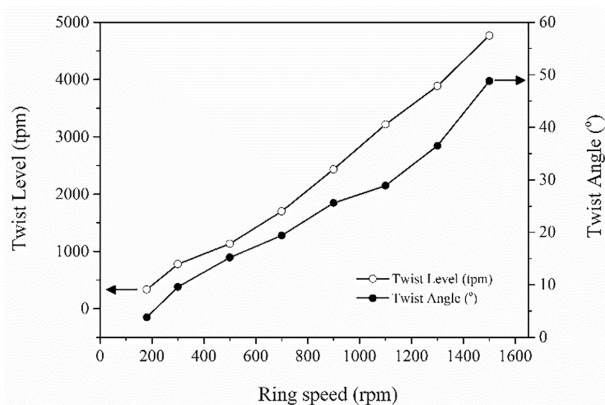


Fig. 6 Effect of ring speed on twist levels and twist angles in nanofibre yarns.

Productivity of nanofibre yarns was determined by winding rate. It was noted that when the winder rate was lower than 90 m/hr, cone apex slacked leading to jerks and yarn breakage. Once the winding rate was above 120 m/hr, a smooth and continuous cone and incessant yarn could be produced. Yarn could be produced without any interruption till speed reached 240 m/hr. Still higher winding rate led to frequent breakages at the cone apex.

The yarn electrospinning under the optimized condition can work continuously. As long as sufficient polymer solution was fed to the two electrospinning systems, yarn was prepared continuously and the yarn diameter had very small change.

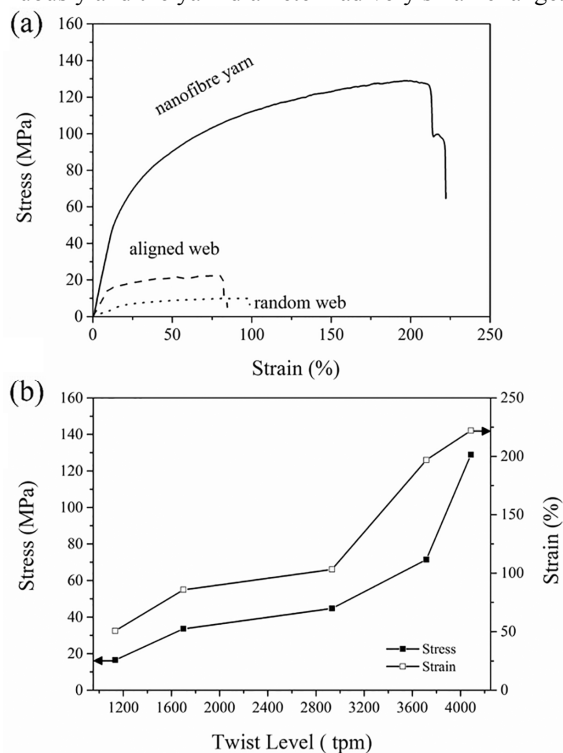


Fig. 7 a) Typical stress ~ strain curves of randomly-orientated nanofibre web, aligned nanofibre web and nanofibre yarn, and b) effect of twist level on yarn tensile and strain values.

The mechanical properties of nanofibre yarn produced from this yarn electrospinning system were evaluated using FAVIMAT (AI) + Robot 2. A gauge length of 10 mm and a vertical jaw speed of 10 mm/min were employed to test at least 5 samples for each category. Samples produced from random and aligned web produced under same conditions were also tested for comparison.

The nanofibre yarn showed a tensile strength and elongation at break of 128.9 MPa and 222.1%, respectively. While randomly orientated and aligned webs had a tensile strength of 9.9 MPa and 22.5 MPa with an elongation at break 98.7 % and 84.6% respectively (Fig. 7a). Yarns prepared with different twist levels were also evaluated. Increasing the twist levels improved tensile strengths and strain values (Fig. 7b). This can be explained by that increasing twists in the yarns enhanced inter-fibre interaction, which strengthening friction between the fibres. Consequently, number of fibres per yarn cross section was increased, increasing the overall tensile strength.

## Conclusions

A novel nanofibre yarn electrospinning system has been developed. The system combines both needle and needleless electrospinning techniques and a ring collector, which can produce continuous bead-free nanofibre yarn with nanofibre and yarn diameter respectively in the range of 541 nm to 1.6  $\mu\text{m}$  and 52  $\mu\text{m}$  to 206  $\mu\text{m}$ , respectively. The yarns have a twist level up to 4,700 twists per metre and productivity up to 240 m/h. The position of the electrospinning units is a crucial parameter affecting nanofibre deposition, fibrous cone stability and yarn production. The nanofibre yarn produced is much higher than that of aligned and nonwoven webs. The novel yarn spinning technique may open up wide applications of nanofibre yarns in various areas.

## Notes and references

Institute for Frontier Materials, Deakin University, Geelong, VIC 3216, Australia; email: [tong.lin@deakin.edu.au](mailto:tong.lin@deakin.edu.au)

1. P. Gibson, H. Schreuder-Gibson and D. Rivin, *Colloids and Surfaces A: Physicochemical and Engineering Aspects*, 2001, **187**, 469-481.
2. X. Wang, Y. G. Kim, C. Drew, B. C. Ku, J. Kumar and L. A. Samuelson, *Nano Letters*, 2004, **4**, 331-334.
3. B. Ding, M. Yamazaki and S. Shiratori, *Sensors and Actuators B: Chemical*, 2005, **106**, 477-483.
4. R. Luoh and H. T. Hahn, *Composites Science and Technology*, 2006, **66**, 2436-2441.
5. W. J. Li, C. T. Laurencin, E. J. Catterson, R. S. Tuan and F. K. Ko, *Journal of Biomedical Materials Research*, 2002, **60**, 613-621.
6. H. Wu, J. Fan, C.-C. Chu and J. Wu, *Journal of Materials Science: Materials in Medicine*, 2010, **21**, 3207-3215.
7. H. Schreuder-Gibson, P. Gibson, K. Senecal, M. Sennett, J. Walker, W. Yeomans, D. Ziegler and P. P. Tsai, *Journal of Advanced Materials*, 2002, **34**, 44-55.

## ARTICLE

8. M. Kosal, *Applying Nanotechnology to Revolutionary Chemical and Biological Countermeasures Nanotechnology for Chemical and Biological Defense*, Springer New York, 2009.
9. S. W. Choi, S. M. Jo, W. S. Lee and Y. R. Kim, *Advanced Materials*, 2003, **15**, 2027-2032.
10. K. Gao, X. Hu, C. Dai and T. Yi, *Materials Science and Engineering: B*, 2006, **131**, 100-105.
11. J. Li, H. Xie, Y. Li and J. Wang, *Journal of Nanoscience and Nanotechnology*, 2013, **13**, 1132-1135.
12. T. Ondarçuhu and C. Joachim, *Europhysics Letters*, 1998, **42**, 215-220.
13. C. R. Martin, *Journal of the American Chemical Society*, 1990, **112**, 8976-8977.
14. P. X. Ma and R. Zhang, *Journal of Biomedical Materials Research*, 1999, **46**, 60-72.
15. E. P. S. Tan and C. T. Lim, *Applied Physics Letters*, 2004, **84**, 1603-1605.
16. X. P. Yang, X. L. Li, L. Zhang, Q. F. Yang, Q. Cai and X. L. Deng, *Polymers for Advanced Technologies*, 2011, **22**, 1078-1082.
17. R. T. Weitz, L. Harnau, S. Rauschenbach, M. Burghard and K. Kern, *Nano Letter*, 2008, **8**, 1187-1191.
18. K. Sarkar, C. Gomez, S. Zambrano, M. Ramirez, E. de Hoyos, H. Vasquez and K. Lozano, *Materials Today*, 2010, **13**, 12-14.
19. A. W. Fahmi, H. Bruenig, R. Weidisch and M. Stamm, *Macromolecular Materials and Engineering*, 2005, **290**, 136-142.
20. C. J. Ellison, A. Phatak, D. W. Giles, C. W. Macosko and F. S. Bates, *Polymer*, 2007, **48**, 3306-3316.
21. K. Nakata, K. Fujii, Y. Ohkoshi, Y. Gotoh, M. Nagura, M. Numata and M. Kamiyama, *Macromolecular Rapid Communications*, 2007, **28**, 792-795.
22. E. S. Medeiros, G. M. Glenn, A. P. Klamczynski, W. J. Orts and L. H. C. Mattoso, *Journal of Applied Polymer Science*, 2009, **113**, 2322-2330.
23. K. T. Guan, X. P. Zhuang, G. L. Yan and B. W. Cheng, *Advanced Materials Research*, 2011, **332**, 1339-1342.
24. J. E. Oliveira, E. A. Moraes, R. G. F. Costa, A. S. Afonso, L. H. C. Mattoso, W. J. Orts and E. S. Medeiros, *Journal of Applied Polymer Science*, 2011, **122**, 3396-3405.
25. Y. Chen, Z. L. Wang, J. S. Yin, D. J. Johnson and R. H. Prince, *Chemical Physics Letters* 1997, **272**, 178-182.
26. V. I. Merkulov, D. H. Lowndes, Y. Y. Wei, G. Eres and E. Voelkl, *Appl. Phys. Lett.*, 2000, **76**, 3555-3557.
27. S. A. Manafi and S. H. Badiee, *Research Letters in Materials Science*, 2008, **2008**, 850975.
28. T. D. Xiao, E. R. Strutt, M. Benaissa, H. Chen and B. H. Kear, *Nanostructured Materials*, 1998, **10**, 1051-1061.
29. S. Nair, M. Tsapatsis, L. A. Villaescusa and M. A. Cambor, *Chemical Communications*, 1999, 921-922.
30. S. Supothina, R. Rattanakam and S. Tawkaew, *Journal of Nanoscience and Nanotechnology*, 2012, **12**, 4998-5003.
31. J. Zheng, Y. Z. Long, B. Sun, H. D. Zhang, J. C. Zhang and J. Y. Huang, *Advanced Materials Research*, 2013, **690-693**.
32. H. W. He, Y. Y. Huang, W.-P. Han, G. F. Yu, X. Yan, Y. Z. Long and L. H. Xia, *Journal of Materials Chemistry C*, 2014, **2**, 8962-8966.
33. U. Ali, Y. Zhou, X. Wang and T. Lin, in *Nanofibers-production, properties and functional applications*, ed. T. Lin, InTech, 2011, ch. 8, pp. 153-174.
34. M. N. Shukat and T. Lin, *Journal of Nanoscience and Nanotechnology*, 2014, **14**, 1389-1408.
35. M. S. Khil, S. R. Bhattarai, H. Y. Kim, S. Z. Kim and K. H. Lee, *Journal of Biomedical Materials Research Part B: Applied Biomaterials*, 2005, **72B**, 117-124.
36. E. Smit, U. Büttner and R. D. Sanderson, *Polymer*, 2005, **46**, 2419-2423.
37. W.-E. Teo, R. Gopal, R. Ramaseshan, K. Fujihara and S. Ramakrishna, *Polymer*, 2007, **48**, 3400-3405.
38. M. Yousefzadeh, M. Latifi, W. E. Teo, M. Amani - Tehran and S. Ramakrishna, *Polymer Engineering & Science*, 2011, **51**, 323-329.
39. Dabirian, F., Hosseini, Y., Ravandi and S. A. Hosseini, *Journal of the Textile Institute*, 2007, **98**, 237 - 241.
40. Dabirian, F., Hosseini and S. A., *Fibres and Textiles in Eastern Europe*, 2009, **74**, 45-47.
41. X. Wang, K. Zhang, M. Zhu, H. Yu, Z. Zhou, Y. Chen and B. S. Hsiao, *Polymer*, 2008, **49**, 2755-2761.
42. U. Ali, X. Wang and T. Lin, *AATCC Review*, 2012, **103**, 57-63.
43. U. Ali, Y. Q. Zhou, X. G. Wang and T. Lin, *Journal of the Textile Institute*, 2012, **103**, 80-88.
44. J. He, K. Qi, Y. Zhou and S. Cui, *Journal of Applied Polymer Science*, 2014, **131**, 40137.
45. J. X. He, K. Qi, Y. M. Zhou and S. Z. Cui, *Polymer International*, 2014.
46. A. Yarin and E. Zussman, *Polymer*, 2004, **45**, 2977-2980.
47. O. Dosunmu, G. Chase, W. Kataphinan and D. Reneker, *Nanotechnology*, 2006, **17**, 1123.
48. J. Varabhas, G. Chase and D. Reneker, *Polymer*, 2008, **49**, 4226-4229.
49. O. Jirsak and S. Petrik, 2010.
50. X. Wang, H. Niu, X. Wang and T. Lin, presented in part at the Textile Research Symposium (38th : 2009 : Susono City, Japan) Susono City, Japan 3-5 Sep. 2009 2009
51. *United States Pat.*, 2011.
52. H. Niu, X. Wang and T. Lin, in *Nanofibers-Production, Properties and Functional Applications. InTech*, 2011, ch. 2, pp. 17-36.
53. H. Niu, X. Wang and T. Lin, *Journal of the Textile Institute*, 2012, **103**, 787-794.
54. P. Pokorný, E. Kostakova, F. Sanetrik, P. Mikes, J. Chvojka, T. Kalous, M. Bilek, K. Pejchar, J. Valtera and D. Lukas, *Physical Chemistry Chemical Physics*, 2014, **16**, 26816-26822.
55. H. Niu, T. Lin and X. Wang, *Journal of Applied Polymer Science*, 2009, **114**, 3524-3530.